Fault Diagnosis of Harmonic Reducers Used in Industrial Collaborative Robots via DWT, MB-FFT, EMD and Machine Learning Classifiers (RF, XGBoost, SVM and KNN)

Samuel Ayankoso[1], Huanqing Han[2], Hamidreza Fahham[3], Gareth Tucker[4], Helen Miao[5] and Fengshou Gu[6]

[1,5,6] Center for Efficiency and Performance Engineering University of Huddersfield, *Huddersfield, UK*
samuel.ayankoso@hud.ac.uk
H.Miao@hud.ac.uk
f.gu@hud.ac.uk

[2] Beijing Institute of Technology, Zhuhai, China
Center for Efficiency and Performance Engineering University of Huddersfield
huanqing.han@hud.ac.uk

[3,4] Institute of Railway Research, University of Huddersfield, *Huddersfield, UK*
h.faham@hud.ac.uk
G.J.Tucker@hud.ac.uk

ABSTRACT

Harmonic reducers are critical components in industrial collaborative robot joints but are prone to faults because they operate under cyclic motion and fluctuating load conditions. This work focuses on three representative failure modes in harmonic reducers: gear tooth of the flexspline breakage, flexible bearing outer race defects, and wear at the flexspline–circular spline interface. To enhance weak fault signatures, three signal preprocessing schemes are evaluated: Discrete Wavelet Transform (DWT), Multiband Fast Fourier Transform (MB-FFT), and Empirical Mode Decomposition (EMD), followed by the extraction of 11 time-frequency domain features from each processed signal set. The resulting features are used to train four classical Machine Learning (ML) classifiers, Random Forest, Extreme Gradient Boosting (XGBoost), Support Vector Machine (SVM) and K-Nearest Neighbors (K-NN). Experimental results show that the proposed MB-FFT technique provides the lowest computational cost while delivering superior classification performance, achieving 100% accuracy when combined with random forest and XGBoost for both vibration and current signals. Compared with deep learning models, the results demonstrate that signal enhancement can significantly improve classification performance despite weak fault characteristics, and that current signals can serve as effective indicators for harmonic drive fault diagnosis in cobots.

1. INTRODUCTION

As we transition to Industry 5.0, where human-robot collaboration is shaping the industrial narrative, industrial collaborative robots (i.e., cobots) stand at the frontier of this evolution. The most commonly used transmission system in cobots is the harmonic reducer, which is valued for its high transmission accuracy and torque, compact size, lightweight design, and low backlash (Guida et al. 2024). However, harmonic reducers can develop various faults, such as flexspline wear, flexspline tooth breakage, and wave generator eccentricity, primarily due to extended operational periods or extreme operating conditions such as high load or torque (Li et al. 2024). These faults can lead to reduced positioning accuracy and excessive vibration. Hence, it is important to develop a robust fault diagnosis model to enhance the reliability and safety of cobots.

Vibration sensing is the most commonly used and effective method for detecting mechanical faults in many machines and components (Chu et al. 2024; Lei et al. 2025), including harmonic reducers. However, most cobots do not come equipped with vibration sensors and adding them incurs additional hardware costs and system complexity. A more practical alternative is to use current signals, which are readily available from the robot controller without requiring additional sensors. However, a significant challenge arises: Deep Learning (DL) models typically perform poorly when using current signals, especially for detecting weak mechanical faults (Ayankoso et al. 2024). This limitation highlights the need for effective signal processing

techniques and Machine Learning (ML) approaches that can extract meaningful fault features from current signals and bridge the gap between performance and practical deployment in industrial cobot systems.

In many studies, DL models have excelled in the fault diagnosis of industrial robot reducers. For example, the detection of a harmonic reducer fault under varying conditions was investigated by Zhi et al. (2022) using a joint wavelet regional correlation threshold denoising algorithm for the suppression of noise in raw vibration sensor data and a Convolutional Neural Network-Long Short-Term Memory (CNN-LSTM) as the classifier. The faults examined are six in total, namely, rigid gear, flexispline teeth fracture, teeth bruise, wave generator misalignment, half broken bearing outer ring, and bearing misalignment. The model achieved a classification accuracy of 94.0%, which surpassed the classification accuracy of other traditional models like CNN, LSTM and Support Vector Machine (SVM). In addition, the fault diagnosis of an RV reducer was examined by using vibration signals and an enhanced convolutional capsule network by Xu et al. (2022). The faults simulated are multitooth sun and planetary gears wear of different degrees, and the proposed method effectively distinguished these compound faults.

Furthermore, the in-situ fault diagnosis of a harmonic reducer was carried out by using Multi-Scale Mixed Convolutional Neural Networks (MSCNN) in the studies by (He et al. 2023). The model was able to extract important fault features from the multichannel signals used, and gear-related faults from different joints characterised by abnormal sound and abnormal rotation were detected. The MSCNN model gave a better accuracy compared to other models like multilayer perceptron, 1D CNN, LSTM-CNN and other state-of-the-art DL methods. Additionally, the use of a Multichannel Hybrid Attention Mechanism (MCHAM) and a Bidirectional Gate Recurrent Unit (BiGRU) was proposed in dealing with harmonic reducer flexispline wear and other faults by Li et al. (2024). The MCHAM part was claimed to be responsible for reducing noise and irrelevant information in the vibration signals used, while the BiGRU captured the feature information from different time series inputs passed down to it. Their results showed that the proposed model is robust in detecting each fault (with an accuracy >97%) under different speeds, loads and intense noise.

The previously reported studies on harmonic reducer fault diagnosis have predominantly relied on vibration signals for model development; however, Raouf et al. (2022) demonstrated the viability of motor current signatures in their work. They addressed two key reasons why current signals are not usually utilised: (1) reducer faults are mostly mechanical; therefore, vibration signals tend to be a better choice, (2) current signal analysis is more complicated because the signals originate from electric motors, which are themselves susceptible to faults. Nonetheless, they presented an approach based on feature extraction, feature reduction, and ML fault classification using Naïve Bayes, SVM, K-Nearest Neighbors (KNN) and ensemble subspace. The results obtained showed that the use of the current signature is effective in the detection of mechanical faults. However, a key limitation of their work is that the proposed ML pipeline, which extracts features directly from the current waveform, is not sufficiently effective, particularly in situations where the examined faults are not severe.

Actually, ML approaches, combining signal enhancement, feature extraction and classical classifiers, were found superior to DL models, mainly due to the use of small/medium datasets and noisy or weak signals, as reported in (Briza et al. 2024; Ayankoso et al. 2024). Building on these findings, this study extends prior work by investigating the integration of additional signal enhancement techniques within classical machine learning pipelines for harmonic reducer fault diagnosis. Given the limited attention to current-based diagnosis, both vibration and current signals are analysed independently to establish comprehensive performance benchmarks. The main contributions of this work are as follows:

1. Systematic evaluation of three advanced signal preprocessing methods, namely Discrete Wavelet Transform (DWT), Multiband Fast Fourier transform (MB-FFT), and Empirical Mode Decomposition (EMD), for extracting discriminative features from vibration and motor current signals collected from a harmonic reducer test bench under diverse conditions.
2. Comprehensive comparative analysis of vibration signals (obtained very close to the fault's location on the test rig) versus current signals (obtained from a motor which is far from the fault source) through an ML pipeline, including feature extraction and evaluation of four classifiers: Random Forest (RF), SVM, Extreme Gradient Boosting (XGBoost), and KNN

The rest of the paper is structured as follows: the methodology of the research is presented in Section 2. The experiment and data analysis are included in Section 3. Sections 4 and 5 cover model development, the results obtained and discussions. The last section (section 6) gives a summary of the study and outlook of the next phase of this study.

2. METHODOLOGY

The methodology adopted in this research is illustrated in Figure 1. Experiments were conducted on a test rig to acquire vibration and current signals. The signals were independently enhanced using three techniques, followed by feature extraction, and the resulting features were used to train four classifiers.

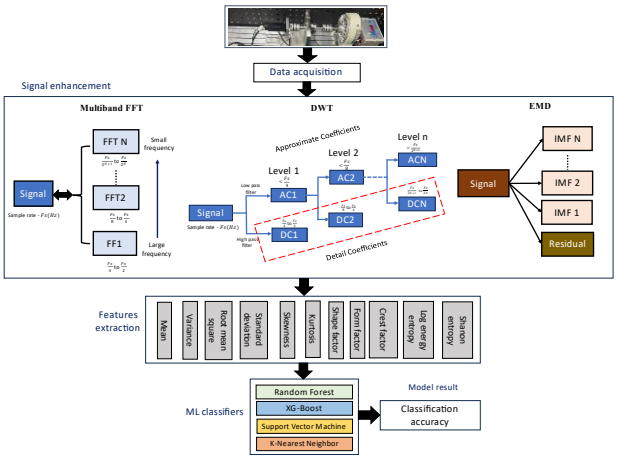

Figure 1. Methodology

2.1. Signal Processing

Three signal preprocessing techniques (DWT, MB-FFT, and EMD) are discussed in this subsection. These three techniques are investigated to evaluate the optimal preprocessing strategy in terms of performance and computational cost.

2.1.1. DWT

DWT is a signal preprocessing technique that decomposes a signal into time-frequency components. This technique is suitable for non-stationary signals, and the decomposition is performed through mathematical functions called wavelets. Wavelets are finite-duration, decaying oscillatory functions (called mother wavelets) that are dilated and shifted to capture transients, sharp discontinuities, and localised, multi-resolution, non-stationary features within signals. The commonly used mother wavelets are Symlets, Daubechies, Haar, Morlet, Mexican-Hat, Gaussian, Biorthogonal and Coiflets (Dey 2021; Das and Bagci Das 2023).

DWT decomposition produces approximation coefficients (low-frequency components) and detail coefficients (high-frequency components) across multiple scales, as shown in Figure 2. Mathematically, a signal $X(t)$ gets decomposed into j levels, wherein each level of the signal is represented by detail ($D_i(t)$) and approximation ($A_i(t)$) coefficients as follows:

$$X(t) = \sum_{i=1}^{j} D_i(t) + A_i(t)\,, \quad (1)$$

$$A_i(t) = \sum_{k=-\infty}^{\infty} x[k]g[2t-k], \quad (2)$$

$$D_i(t) = \sum_{k=-\infty}^{\infty} x[k]h[2t-k], \quad (3)$$

where g is a low-pass filter (scaling function), h is a high-pass filter (which also represents the wavelet function), and k is the shift index that moves the wavelet along the time axis.

The detail coefficients describe the high-frequency content of the signal, capturing transient or impulsive signal variations that typically indicate fault events. Statistical properties or energy distributions of these detail coefficients yield discriminative features for fault classification. Moreover, the approximate and detailed coefficients at each level have specific frequency bands they represent. The frequency range of the approximate coefficients is $\left[0 - \frac{Fs}{2^{i+1}}\right]$ while that of the detail coefficients is $\left[\frac{Fs}{2^{i+1}} - \frac{Fs}{2^{i}}\right]$ (Abdulhady Jaber and Bicker 2020).

Not all detail coefficients contribute meaningfully to fault discrimination; many of them capture noise or irrelevant signal content. Feature selection techniques can identify the most discriminative coefficients; thus, reducing feature space dimensionality while improving classification accuracy and model robustness.

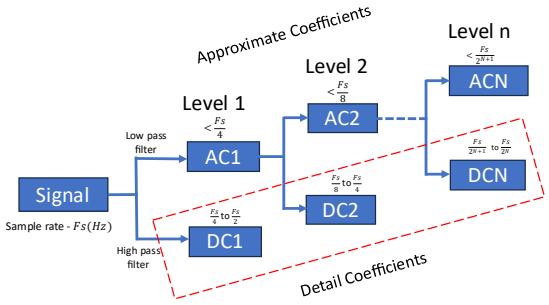

Figure 2. DWT

2.1.2. Multiband FFT

The discrete Fourier transform involves using the FFT algorithm to convert a sequence of discrete time-domain samples into its frequency-domain representation. FFT is a popular and long-existing tool for analysing stationary signals (i.e., signals with unchanging spectral information over time). FFT decomposes a signal into a linear combination of sinusoids (sines and cosines) at discrete frequencies. The resulting frequency spectrum displays the amplitude and phase of each sinusoidal component present in the input signal.

Mathematically, FFT transforms the analysed waveform *X(t)* with *t* samples into the frequency domain and the expression for that is presented in Eq. (4).

$$Y(f) = \int_{-\infty}^{\infty} X(t)e^{-2i\pi ft}dt, \quad (4)$$

where, $e^{-2i\pi ft} = \cos(2\pi ft) + i\sin(2\pi ft)$.

Specific fault signatures or defects can be identified by examining the frequency spectrum. Various features can be extracted from the FFT spectrum to characterise faults, including the amplitude of specific frequency peaks, the presence of harmonics or sidebands, spectral energy distribution, or other relevant spectral metrics. For example, the harmonics, characterising integer multiples of the natural (f_0) of an induction motor, were used to form the

features used in distinguishing two mechanical faults from a normal healthy state in the work of (Ayankoso et al. 2024). However, the presence of clear harmonics cannot be guaranteed in some signals, and the selection of the peak points isn't very precise; hence, a multiband FFT approach is proposed based on the multiscale frequency bands generated by DWT, as displayed in Figure 3.

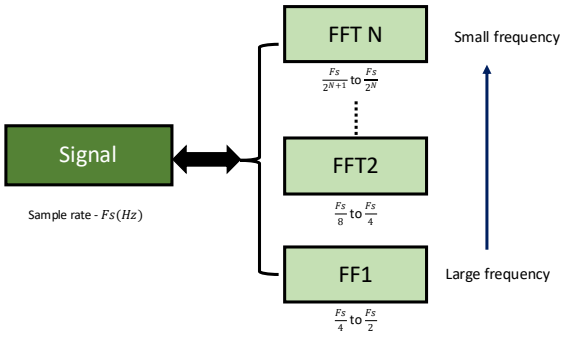

Figure 3. Multiband FFT

2.1.3. EMD

Empirical Mode Decomposition is used in preprocessing nonlinear and non-stationary signals by breaking the signal down into locally meaningful finite numbers of oscillatory components, also called Intrinsic Mode Functions (IMFs). A signal can be regarded as an IMF if the following two conditions are met (Patel and Shakya 2020):

a. The difference between the number of extreme values and the number of all the zero crossings in the signal is either zero or one.
b. At any point, the mean value of the envelope formed by the local minima and the local maxima is zero.

Mathematically, a signal (X) which is a function of time, can be decomposed into (Wang et al. 2021):

$$X(t) = \sum_{i=1}^{n} I_i + R_n, \quad (5)$$

where, I_i represents the intrinsic mode function, n is the total number of IMFs, while R is the residual.
Splines such as cubic splines are used in the EMD algorithm as the interpolation method to construct the upper and lower envelopes during the sifting process. Figure 4 shows the outputs of decomposing a signal into N levels using EMDs

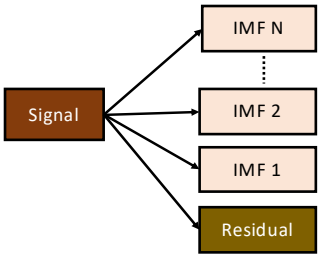

Figure 4. EMD

2.2. Feature Extraction

Feature extraction in ML involves transforming raw or processed data into a simplified and informative set of numerical features capturing the most relevant information to help in faster computation, better accuracy and reduced risk of overfitting by filtering out noise and irrelevant information in signals. There are different statistical features that can be extracted from a time or frequency domain signal. An example is the RMS, which shows the average power of a signal. Further details about the time and frequency domain features used in the fault diagnosis of rotating machinery can be found in (Sánchez et al. 2024).

2.3. ML Classifiers

Four classic classifiers are investigated in this research, and they are RF, XGBoost, KNN and SVM.

2.3.1. RF

Random forest belongs to the type of ensemble ML technique where random samples and features are used in generating diverse decision trees, with each tree predicting the fault class, and the final prediction is done via majority voting. Mathematically, RF builds T number of decision trees and the algorithm output is C_{pred} (Pohakar et al. 2025).

$$C_{pred} = \arg\max_{c_p} \sum_{t=1}^{T} I(C_t(x) = c_p) \quad (6)$$

where, $C_t(x)$ is the class of fault predicted by tree t, c_p denotes the fault types of the case study, while $I(C_t(x) = c_p)$ represent a function that indicates if the prediction by tree t is true or false (it returns 1 for true and 0 for false).

RF is a robust technique that addresses fault diagnosis problems with higher-dimensional data and is able to prevent overfitting. One major challenge with RF is interpretability, particularly as the number of trees generated increases (Yang and Wang 2025).

2.3.2. XGBoost

The XGBoost model also belongs to the ensemble classification approaches. It works by building trees sequentially, with every new tree causing an improvement to the model by reducing the error emanating from the iterations. XGBoost's effectiveness primarily arises from its objective function, which integrates a loss term with regularisation, helping to prevent overfitting and underfitting issues (Kim et al. 2023; Tuyet-Doan et al. 2025). The minimised function $(\mathcal{L})$ is computed as:

$$\mathcal{L} = \sum_{i=1}^{N} l(y_i, \hat{y}_i) + \sum_{k=1}^{K} \Omega(f_k), \quad (7)$$

$$\Omega(f_k) = \gamma Q + \frac{1}{2}\lambda\|\omega\|^2, \quad (8)$$

where $l(y_i, \hat{y}_i)$ represents the loss between the true label and the prediction, while $\Omega(f)$ is the regularisation term. In

the regularisation term, f_k is the kth tree, Q represents the count of leaf nodes in the tree, while ω denotes the weight assigned to each leaf node. The constants γ and λ serve as regularisation parameters.

2.3.3. SVM

SVM is a commonly used ML technique for classification problems such as the classification of gear faults. The SVM core idea is about finding the best hyperplane that maximally separates the nearest datapoints in two opposing classes (Tun et al. 2021). Using this approach, the algorithm finds the optimal decision boundary between two or more classes and enables it to generalise well when exposed to new data. When the data is linearly separable, the optimisation problem is as follows:

$$\underset{\omega,b}{\text{minimize}} \ \ \frac{1}{2}\|\omega\|^2, \tag{9}$$

subject to $y_i(\omega^T x_i + b) \geq 1, \ \forall\, i = 1, \ldots \ldots, n.$

where ω is the weight vector, b is the bias term, y_i is the label for each class, and x_i represents the feature vector.

SVM can be applied to linear and nonlinear problems. When data provided cannot be separated in a linear form, kernel functions are employed to change the original data into a higher-dimensional space for easier separation. Some kernel functions are polynomial kernels, sigmoid kernels and radial basis functions (Almatheel and Osman 2021). Besides, slack variables and cost parameters are added to the objective function formulation for nonlinearly separable data. Though SVM is very effective in multiple-class separation, the performance may degrade when the data used is imbalanced (Yang and Wang 2025).

2.3.4. KNN

The KNN algorithm is very simple, and it works by finding the K-nearest training data points in the feature space to predict a new sample data point. The class prediction is based on the majority class. The metrics used in computing the nearest neighbour include Euclidean distance, Manhattan distance and Minkowski distance (Pohakar et al. 2025). The Euclidean distance between a test sample X and X_i is:

$$D(X, X_i) = \sqrt{\sum_{j=1}^{n}(x_j - x_{ij})^2}, \tag{10}$$

where x_j and x_{ij} correspond to the feature of the training and test samples, respectively, while n indicates the number of features.

The major drawback of this algorithm is that it can be computationally intensive, especially when dealing with multichannel industrial datasets (Yang and Wang 2025).

3. EXPERIMENTS AND DATA ANALYSIS

In the manufacturing of industrial robots, three main types of gears are commonly used; they are harmonic drive, rotary vector (RV) reducer and planetary gear (Li et al. 2024). In cobot applications, harmonic drives offer unique benefits over RV reducers because of their smaller size, lighter weight, and superior precision. A harmonic drive consists of a wave generator (WG), flexspline (FS), and circular spline (CS). A WG is an elliptically shaped cam inserted inside a deformable ball bearing and has a hole for connecting the motor. FS houses the WG; it has a thin wall and an external gear that meshes with the internal teeth of the CS while transferring motion. Harmonic drives are susceptible to multiple types of failures due to their complex elastic deformation mechanism and unique meshing characteristics. In this case study, the fault diagnosis of a harmonic drive is investigated, as this component is prone to wear and tooth breakage from the continuous, repetitive motion of collaborative robots.

3.1. Experiment

The experimental platform used for acquiring data from normal and faulty harmonic drives is shown in Figure 5. It consists of three main subsystems: a drive system (comprising a servo motor, drive unit, and controller), the harmonic drive unit under test, and a loading system featuring a magnetic powder brake with a tension controller. The data acquisition system utilises a YMC unit and records signals of vibration around the drive and the motor current.

The faults considered are tooth breakage, flexible bearing outer race fault and artificially induced wear. The first fault was created by artificially inducing a tooth surface breakage on the flexipline. The second fault was created by machining a hole into the flexible bearing outer race, which connects to the wave generator. Lastly, a wear fault was simulated using diamond grinding paste (i.e., a wear-accelerating substance) injected into the meshing interface between the flexspline and circular spline. The paste contained 5 μm particles. As shown in Table 1, the dataset created during the experiments conducted includes a normal/baseline experiment repeated at three different speeds and the three faults were also repeated at those speeds. The operating speeds are 600 rpm, 1200 rpm and 1800 rpm, while the operating loads are 0 A load and 0.4 A load. The signals measured during each experiment are vibrations from an accelerometer near the drive and current from the motor supply. Each of the baseline experiments, including each of the fault experiments, was done in 3 minutes with a sampling frequency of 50 kHz.

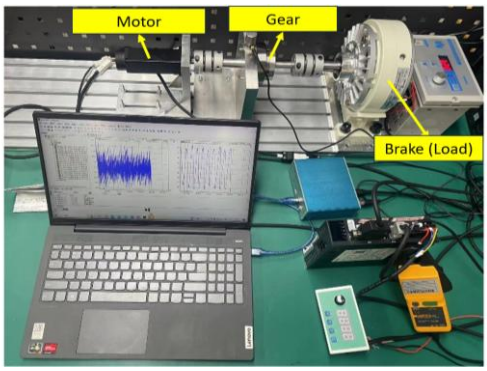

Figure 5. Harmonic drive test bench

Table 1. Parameters used during experiments

Parameters	Value
Fault type/class	Normal, Bearing, Flexspline tooth breakage, Wear
Experiment time	3 minutes
Sample frequency	50 kHz
Speed	600/1200/1800 $\boldsymbol{rpm}$
Load current of the powder brake	0 A, 0.4A

3.2. Data Analysis

The vibration and current signals obtained from the experiments conducted are plotted in Figures 6 and 7. The first 500 data points of the vibration signals and the first 5000 data points of the current signals are shown in order to have a much closer look at the data based on the operating conditions. In addition, the RMS plot of both signals can be seen in Figure 8. There is an observable difference or pattern in the RMS calculated for the normal condition and fault cases when the vibration signals are examined. Besides, the current signals' RMS calculation also showed a similar pattern, but the magnitude of change in RMS with respect to each fault and other operating conditions is not as high as that of the vibration signals.

4. DATA SPLIT, SIGNAL PROCESSING METHODS AND ML MODELS IMPLEMENTATION

This section describes the implementation steps for the signal preprocessing methods considered, as well as the ML models trained and evaluated on an Intel Core i7-13800H CPU, 32 GB RAM, using the experimental data.

4.1. Data Split

Two datasets were constructed from the acquired experimental data, namely a train-validation set and a test set. The first two minutes of the signals under each operating condition were used to form the training validation set, while the remaining one minute was reserved for testing. Each dataset was further segmented using a window length of 50,000 samples with a stride of 50,000. As a result, each fault class comprised 357 segments of length 50,000 in the train-validation set and 117 segments of the same length in the test set.

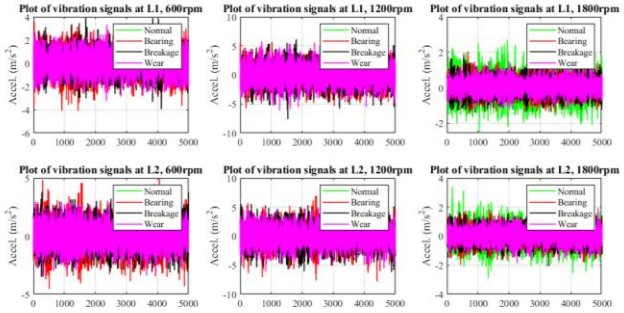

Figure 6. Vibration data for the baseline and fault states

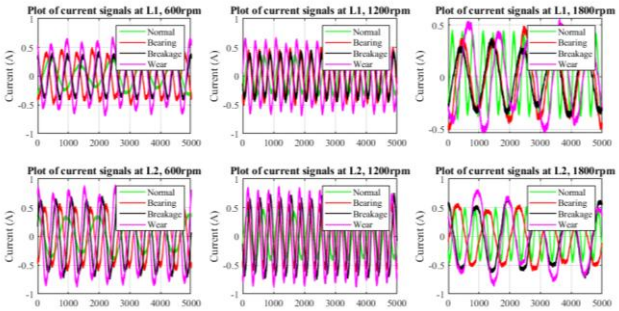

Figure 7. Current data for the baseline and fault states

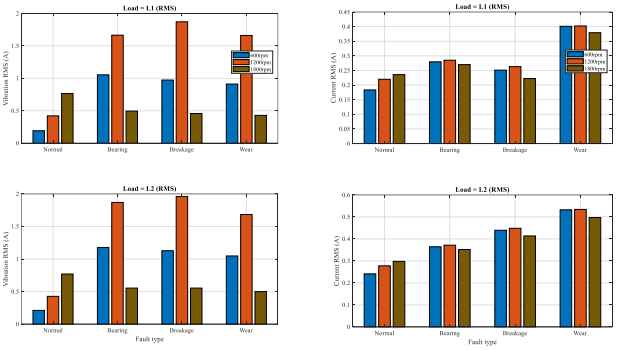

Figure 8. Vibration and current data RMS for the three faults and baseline experiments

4.2. Signal processing methods Implementation

The three signal preprocessing methods, DWT, MB-FFT and EMD, were executed in Python, and 11 features were extracted from the resulting signals based on each method. The features extracted include mean, variance, standard deviation, root mean square, skewness, kurtosis, shape factor, form factor, crest factor, log energy entropy, and Shannon entropy. The details of each feature, such as their formula and description, can be found in (Ayankoso et al. 2024; Raouf et al. 2022). For the DWT implementation, the

wavedec function in "pywt" library was used, and "db3" wavelet was selected with the decomposition performed up to 4 levels. In (Silik et al.), db3 outperformed other wavelets by showing low mean squared error and high SNR, and also exhibited a good balance between preserving signal energy and representing it sparsely, which informed the selection of db3 as the mother wavelet used. Based on the actual sampling frequency used in the experiment, the frequency bands of each DWT level, as listed in Table 2, were used to compute MB-FFTs. The FFT computation was done using the 'fft' function available in the numpy library, and a frequency-domain bandpass filter was applied directly to the FFT, enforcing that only a specific band of frequencies is retained. For the EMD implementation, the "pyEMD" library in Python was used. The number of IMFs each signal was decomposed into is 4 in order to have a very fair comparison. We also used these two settings for the EMD numerical stability and speed: spline_kind='akima', FIXE=10.

Table 2. Frequency range of each DWT level

Level	Frequency Range (Hz)	Frequency Range Values (Hz)
Level 1	$\frac{Fs}{4}$ to $\frac{Fs}{2}$	12500 - 25000
Level 2	$\frac{Fs}{8}$ to $\frac{Fs}{4}$	6250 - 12500
Level 3	$\frac{Fs}{16}$ to $\frac{Fs}{8}$	3125 - 6250
Level 4	$\frac{Fs}{32}$ to $\frac{Fs}{16}$	1562.5 - 3125

4.3. ML Models Implementation

The RF, XGBoost, SVM and KNN models were trained using three distinct sets of features. The first, second and third sets of features were derived from the transformed signals after performing DWT, MB-FFT and EMD. The total number of features in each set is 44 (11*4 level). Each model's parameter range or type is set based on values from similar studies and subsequently refined through a grid search. The hyperparameters search space used while training the four ML models is listed in Table 3.

Table 3. ML models parameters

Models	Parameters
Random forest	"n_estimators": [200, 500, 800] "max_features": [5, 10, "sqrt", "log2"]
XGBoost	"n_estimators": [100, 300, 500] "max_depth": [3, 5, 7, 10]
SVM	"svc__C": [0.1, 1, 10, 100] "svc__gamma": ["scale", "auto", 0.01, 0.001]
KNN	"n_neighbors": [1, 3, 5, 7, 9] "metric": ["euclidean", "manhattan", "minkowski"]

5. RESULTS AND DISCUSSIONS

The features extracted from the enhanced vibration and current signals were used to train the machine learning models. Unlike the signal processing techniques, which exhibited some randomness when run 10 times, the machine learning models employed fixed random seeds; consequently, the accuracy results obtained across 10 or more runs were identical. The detailed training, test, and validation results of each model with different signal and feature types are presented in Table 4. From the table, it is evident that all four ML models (RF, XGBoost, SVM, KNN) achieve extremely high accuracies for both vibration and current signals after DWT-, MB-FFT-, and EMD-based feature extraction. In particular, MB-FFT-based features yield the best performance, with 100% validation and test accuracy achieved with RF for both vibration and current signals, while DWT-based features with RF show minor drops to 99.85% on test sets. SVM also performs near-perfectly, with only small reductions in test accuracy (still above 99%), especially for current signals with EMD. KNN is slightly weaker, especially on current data with EMD (test accuracy ≈91%), but overall performance remains very strong. These results confirm that classical ML models, when paired with engineered vibration/current features, can almost perfectly solve the fault classification problem in this case study.

The confusion matrices of the best- and worst-performing signal processing techniques (i.e. MB-FFT and EMD) after feature extraction and classification with RF and KNN, using both vibration and current signals, are shown in Figures 9 and 10, respectively. In Figure 9 (a), the MB-FFT features with RF show no misclassifications, whereas in Figure 9 (b), two distinct misclassification patterns appear with the EMD features and KNN: three Bearing-fault samples are predicted as Wear, and two Wear-fault samples are predicted as Bearing. Similarly, in Fig. 10 (a), all samples are correctly classified when MB-FFT features with RF are applied to the current data. However, the confusion matrix in Figure 10 (b) shows that Normal and Breakage faults are frequently confused: 25 Breakage samples are predicted as Normal, and 30 Normal samples are predicted as Breakage. This suggests that the feature patterns of Normal and Breakage are similar, or that their decision boundaries overlap. Additionally, the Bearing and Wear classes are learned very well, with only a few Bearing samples predicted as Normal and no confusion for Wear.

The results in Table 5 show the signal processing times for each method, while Table 6 reports the training and inference times for the RF, XGBoost, SVM, and KNN models. The processing times in Table 6 include the time required to process all samples in both the training and test datasets. Signal processing was repeated 10 times to compute average times for each method, revealing that MB-FFT is the fastest, followed by DWT, whereas EMD requires more than 90 times longer to process the training

data than the other two methods. In Table 6, SVM stands out as the fastest model to train, with the lowest inference time overall. XGBoost has the next-best inference time, but it also has the highest training time.

To gain deeper insights into the model's learning dynamics, we examined the distributions of features generated from both the vibration and current signals after the signal preprocessing and feature extraction. The T-distributed Stochastic Neighbour Embedding (t-SNE) plots of both signals are displayed in Figure 11. The figure depicts that the lower-dimensional representation of the vibration-based features is better than that of the current features, based on lesser overlap and visually clearer boundaries between clusters.

Table 4. The performance of ML models with the vibration and current signals (4 levels and 1s length data analysis)

Signal	Model	DWT + features extraction (%)			MB-FFT + features extraction (%)			EMD + features extraction (%)		
		Training	Val	Test	Training	Val	Test	Training	Val	Test
Vibration	RF	100	100	99.85	100	100	100	100	99.53	100
	XGBoost	100	99.30	99.70	100	100	100	100	99.53	100
	SVM	100	100	99.85	100	99.78	100	100	99.53	99.85
	KNN	100	100	99.70	100	97.90	98.36	100	99.77	99.25
Current	RF	100	100	99.85	100	100	100	100	100	100
	XGBoost	100	100	99.85	100	100	100	100	100	100
	SVM	100	97.67	96.43	100	99.07	98.66	100	99.53	99.26
	KNN	100	99.53	97.17	100	97.90	95.53	100	94.64	91.22

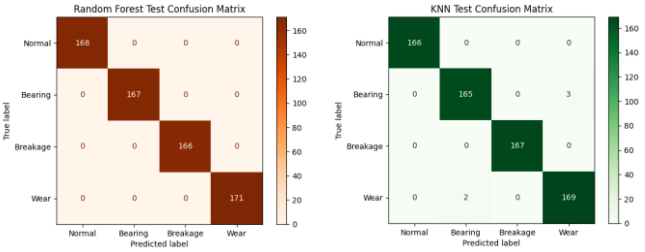

(a) MB-FFT features+RF (b) EMD features+KNN

Figure 9. Confusion matrix produced using vibration signals

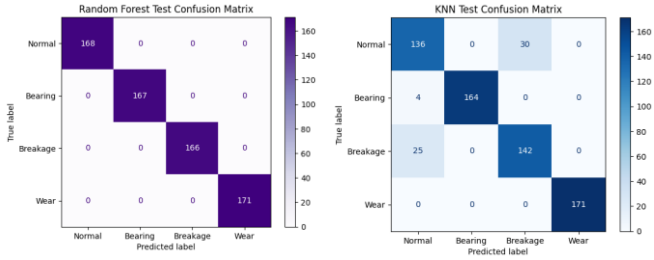

(a) MB-FFT features+RF (b) EMD features+KNN

Figure 10. Confusion matrix produced using current signals

Table 5. Signal processing time of different methods

Signal	Signal processing time (s)		
	DWT	MB-FFT	EMD
Vibration	8.76± 0.74	8.41 ± 0.23	746.99±48.76
Current	8.92 ± 0.21	8.65 ± 0.22	819.29±182.38

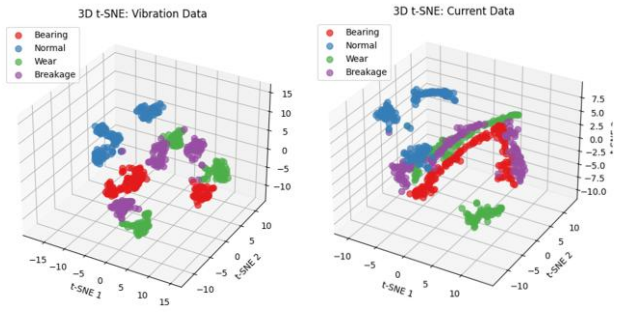

(a) Vibration (b) Current

Figure 11. TSNE-based data visualisation after MB-FFT+ feature extraction

Table 6. Training and inference time of different ML models with the MB-FFT features

Signal	Model	Training time (s)	Inference time (s)
Vibration	RF	6.6009	0.0788
	XGBoost	20.8184	0.0153
	SVM	0.1675	0.0108
	KNN	0.1456	0.9836
Current	RF	7.7185	0.0748
	XGBoost	23.7575	0.0197
	SVM	0.1437	0.0318
	KNN	0.4236	0.0445

Three DL models, namely 1D-CNN, 2D-CNN, and Multiscale 1D-CNN–LSTM, were trained, validated, and tested using the same experimental datasets containing vibration and current signals. For the vibration data, the Multiscale 1D-CNN–LSTM achieved the highest validation and test performance, with accuracies in the range of 75–84%, outperforming both the 1D-CNN and 2D-CNN models. In contrast, the classification accuracies obtained with current signals were substantially lower than those achieved with vibration signals. The misclassification rates exceeded 40% across all three DL models when using current signals. These results indicate that the DL models were unable to extract discriminative features from the raw data of each class. Consequently, this highlights the robustness of the proposed ML pipeline in accurately classifying each fault using both independently examined signal types, particularly when compared to the performance of the DL approaches.

6. CONCLUSION

In conclusion, this study presents a comprehensive ML-based fault diagnosis methodology for harmonic reducers used in industrial collaborative joints, leveraging DWT, MB-FFT, and EMD to enhance weak fault signatures associated with gear breakage, bearing defects, and flexspline wear. The MB-FFT-based features (i.e., the features of the proposed signal processing technique) achieved exceptional diagnostic accuracy, reaching up to 100% with RF and KNN when both vibration and current signals were used. Furthermore, MB-FFT exhibited the lowest computational cost among the three preprocessing methods. The classification accuracy from DWT- and EMD-based features, together with RF and KNN, also achieved 100% or near 100% values. In contrast, the accuracies of SVM and KNN were slightly lower, particularly with the test dataset.

The overall results showed that vibration signals slightly outperformed current signals, with minimal misclassifications observed in the confusion matrices. t-SNE visualisations further corroborate this finding, revealing that vibration-based features form fault clusters that are more distinctly separated than those derived from current signals. Nevertheless, this work demonstrates that current data, which is readily available from the controller, is a good alternative to vibration signals, as it can perform close to vibration signals in detecting the mechanical faults examined. In addition, the ML models performed substantially better than the DL models investigated, as the former leveraged different signal enhancement methods to extract rich, discriminative information from the raw datasets used in this study.

This work has several limitations. A condition-specific stationary dataset was used; the model explainability was not considered, and a more extensive analysis of the extracted features is required to identify the optimal 3 to 5 features for each signal processing technique. Additionally, the robustness test of the ML models against white noise is crucial to evaluate their adaptability to noisy datasets and real-world data variations.

Future work will focus on addressing these limitations and exploring few-shot learning, which is critical for scenarios with scarce labelled fault data, a common challenge in emerging robotic systems. Few-shot learning will enable rapid adaptation with minimal samples, and improve generalisation to unseen and more complex operating conditions

REFERENCES

Abdulhady Jaber, Alaa, and Robert Bicker. 2020. ‘Fault Diagnosis of Industrial Robot Bearings Based on Discrete Wavelet Transform and Artificial Neural Network’. *International Journal of Prognostics and Health Management* 7 (2). https://doi.org/10.36001/ijphm.2016.v7i2.2365.

Almatheel, Yaser Ali, and Mohamed Osman. 2021. ‘Bearing Element Fault Diagnosis Using Support Vector Machine’. *2020 International Conference on Computer, Control, Electrical, and Electronics Engineering (ICCCEEE)*, February 26, 1–5. https://doi.org/10.1109/ICCCEEE49695.2021.9429590.

Ayankoso, Samuel, Ananta Dutta, Yinghang He, Fengshou Gu, Andrew Ball, and Surjya K. Pal. 2024. ‘Performance of Vibration and Current Signals in the Fault Diagnosis of Induction Motors Using Deep Learning and Machine Learning Techniques’. *Structural Health Monitoring*, November 8, 14759217241289874. https://doi.org/10.1177/14759217241289874.

Briza, Antonio C., Eduardo Piedad, and Elmer C. Peramo. 2024. ‘Simpler Machine Learning Methods Outperform Deep Learning in Motor Fault Detection’. *2024 International Conference on Artificial Intelligence in*

Information and Communication (ICAIIC), February, 675–80. https://doi.org/10.1109/ICAIIC60209.2024.10463445.

Chu, Thuy, Tan Nguyen, Hyunsang Yoo, and Jihoon Wang. 2024. 'A Review of Vibration Analysis and Its Applications'. *Heliyon* 10 (5): e26282. https://doi.org/10.1016/j.heliyon.2024.e26282.

Das, Oguzhan, and Duygu Bagci Das. 2023. 'Smart Machine Fault Diagnostics Based on Fault Specified Discrete Wavelet Transform'. *Journal of the Brazilian Society of Mechanical Sciences and Engineering* 45 (1): 55. https://doi.org/10.1007/s40430-022-03975-0.

Dey, Indrakshi. 2021. *Wavelet Transform for IoT – A Signal Processing Perspective*. https://doi.org/10.36227/techrxiv.14560821.v1.

Guida, Roberto, Antonio Carlo Bertolino, Andrea De Martin, and Massimo Sorli. 2024. 'Comprehensive Analysis of Major Fault-to-Failure Mechanisms in Harmonic Drives'. *Machines* 12 (11): 776. https://doi.org/10.3390/machines12110776.

He, Yiming, Jihong Chen, Xing Zhou, and Shifeng Huang. 2023. 'In-Situ Fault Diagnosis for the Harmonic Reducer of Industrial Robots via Multi-Scale Mixed Convolutional Neural Networks'. *Journal of Manufacturing Systems* 66 (February): 233–47. https://doi.org/10.1016/j.jmsy.2022.12.001.

Kim, Min-Chan, Jong-Hyun Lee, Dong-Hun Wang, and In-Soo Lee. 2023. 'Induction Motor Fault Diagnosis Using Support Vector Machine, Neural Networks, and Boosting Methods'. *Sensors* 23 (5): 2585. https://doi.org/10.3390/s23052585.

Lei, Yaguo, Huan Liu, Naipeng Li, Junyi Cao, Yuting Qiao, and Hongbo Wang. 2025. 'Condition Monitoring and Fault Diagnosis of Industrial Robots: A Review'. *Science China Technological Sciences* 68 (1): 1110301. https://doi.org/10.1007/s11431-024-2810-2.

Li, Kai, Ronggang Yang, Tianci Wei, Yiwen Yang, and Jiawei Xiang. 2024. 'Fault Diagnosis of the Harmonic Reducer Based on Dual-Path Convolutional Network with Multi-Channel Hybrid Attention Mechanism'. *Measurement Science and Technology* 36 (1): 016130. https://doi.org/10.1088/1361-6501/ad8179.

Patel, Akash, and Piyush Shakya. 2020. 'Early Fault Detection Based on Empirical Mode Decomposition Method'. *Procedia CIRP* 88: 31–35. https://doi.org/10.1016/j.procir.2020.05.006.

Pohakar, Puja, Ravi Gandhi, Surender Hans, Gulshan Sharma, and Pitshou N. Bokoro. 2025. 'Analysis of Multiple Faults in Induction Motor Using Machine Learning Techniques'. *E-Prime - Advances in Electrical Engineering, Electronics and Energy* 12 (June): 101007. https://doi.org/10.1016/j.prime.2025.101007.

Raouf, Izaz, Hyewon Lee, and Heung Soo Kim. 2022. 'Mechanical Fault Detection Based on Machine Learning for Robotic RV Reducer Using Electrical Current Signature Analysis: A Data-Driven Approach'. *Journal of Computational Design and Engineering* 9 (2): 417–33. https://doi.org/10.1093/jcde/qwac015.

Sánchez, René-Vinicio, Jean Carlo Macancela, Luis-Renato Ortega, Diego Cabrera, Fausto Pedro García Márquez, and Mariela Cerrada. 2024. 'Evaluation of Hand-Crafted Feature Extraction for Fault Diagnosis in Rotating Machinery: A Survey'. *Sensors* 24 (16): 5400. https://doi.org/10.3390/s24165400.

Silik, Ahmed, Mohammad Noori, Wael A. Altabey, Ji Dang, Ramin Ghiasi, and Zhishen Wu. n.d. *Optimum Wavelet Selection for Nonparametric Analysis toward Structural Health Monitoring for Processing Big Data from Sensor Network: A Comparative Study*.

Tun, Wunna, Johnny Kwok-Wai Wong, and Sai-Ho Ling. 2021. 'Hybrid Random Forest and Support Vector Machine Modeling for HVAC Fault Detection and Diagnosis'. *Sensors* 21 (24): 8163. https://doi.org/10.3390/s21248163.

Tuyet-Doan, Vo-Nguyen, Mooryong Choi, and Giseo Park. 2025. 'XGBoost Method-Based Gearbox Fault Diagnosis Using Time-Domain Signal Under Road Vehicle Characteristics'. *Electronics* 14 (23): 4736. https://doi.org/10.3390/electronics14234736.

Wang, Jingyue, Jiangang Li, Haotian Wang, and Lixin Guo. 2021. 'Composite Fault Diagnosis of Gearbox Based on Empirical Mode Decomposition and Improved Variational Mode Decomposition'. *Journal of Low Frequency Noise, Vibration and Active Control* 40 (1): 332–46. https://doi.org/10.1177/1461348420908364.

Xu, Qitong, Chang Liu, Enshan Yang, and Mengdi Wang. 2022. 'An Improved Convolutional Capsule Network for Compound Fault Diagnosis of RV Reducers'. *Sensors* 22 (17): 6442. https://doi.org/10.3390/s22176442.

Yang, Yaqiao, and Hongjun Wang. 2025. 'Random Forest-Based Machine Failure Prediction: A Performance Comparison'. *Applied Sciences* 15 (16): 8841. https://doi.org/10.3390/app15168841.

Zhang, Yuepeng, Jun Wu, Bo Gao, et al. 2025. 'Fault Types and Diagnostic Methods of Manipulator Robots: A Review'. *Sensors* 25 (6): 1716. https://doi.org/10.3390/s25061716.

Zhi, Zhuo, Liansheng Liu, Datong Liu, and Cong Hu. 2022. 'Fault Detection of the Harmonic Reducer Based on CNN-LSTM With a Novel Denoising Algorithm'. *IEEE Sensors Journal* 22 (3): 2572–81. https://doi.org/10.1109/JSEN.2021.3137992.